



Research article

SARS-CoV-2 causes secretory diarrhea with an enterotoxin-like mechanism, which is reduced by diosmectite



Marco Poeta^a, Valentina Cioffi^a, Vittoria Buccigrossi^a, Francesco Corcione^b, Roberto Peltrini^b, Angela Amoresano^c, Fabio Magurano^d, Maurizio Viscardi^e, Giovanna Fusco^e, Antonietta Tarallo^a, Carla Damiano^a, Andrea Lo Vecchio^a, Eugenia Bruzzese^a, Alfredo Guarino^{a,*}

^a Department of Translational Medical Science, Section of Pediatrics, University of Naples Federico II, Naples, Italy

^b Department of Public Health, University of Naples Federico II, Naples, Italy

^c Department of Chemical Sciences, University of Naples Federico II, Naples, Italy

^d Department of Infectious Diseases, National Institute of Health, Rome, Italy

^e Istituto Zooprofilattico Sperimentale Del Mezzogiorno, Portici, Naples, Italy

ARTICLE INFO

Keywords:

COVID-19

Gastroenteritis

Oxidative stress

Diosmectite

ABSTRACT

Background and aims: The pathophysiology of SARS-CoV-2-associated diarrhea is unknown. Using an experimental model validated for rotavirus-induced diarrhea, we investigated the effects of SARS-CoV-2 on transepithelial ion fluxes and epithelial integrity of human intestinal cells. The effect of the anti-diarrheal agent diosmectite on secretion was also evaluated following its inclusion in COVID-19 management protocols.

Methods: We evaluated electrical parameters (intensity of short-circuit current [*I*_{sc}] and transepithelial electrical resistance [TEER]) in polarized Caco-2 cells and in colonic specimens mounted in Ussing chambers after exposure to heat-inactivated (hi) SARS-CoV-2 and spike protein. Spectrofluorometry was used to measure reactive oxygen species (ROS), a marker of oxidative stress. Experiments were repeated after pretreatment with diosmectite, an anti-diarrheal drug used in COVID-19 patients.

Results: hiSARS-CoV-2 induced an increase in *I*_{sc} when added to the mucosal (but not serosal) side of Caco-2 cells. The effect was inhibited in the absence of chloride and calcium and by the mucosal addition of the Ca²⁺-activated Cl⁻ channel inhibitor A01, suggesting calcium-dependent chloride secretion. Spike protein had a lower, but similar, effect on *I*_{sc}. The findings were consistent when repeated in human colonic mucosa specimens. Neither hiSARS-CoV-2 nor spike protein affected TEER, indicating epithelial integrity; both increased ROS production. Pretreatment with diosmectite inhibited the secretory effect and significantly reduced ROS of both hiSARS-CoV-2 and spike protein.

Conclusions: SARS-CoV-2 induces calcium-dependent chloride secretion and oxidative stress without damaging intestinal epithelial structure. The effects are largely induced by the spike protein and are significantly reduced by diosmectite. SARS-CoV-2 should be added to the list of human enteric pathogens.

1. Introduction

SARS-CoV-2 is recognized as a lung-tropic virus, but a substantial number of patients with COVID-19 experience a range of gastrointestinal (GI) symptoms, including anorexia, nausea, vomiting, diarrhea, and abdominal pain [1]. Diarrhea is the most common SARS-CoV-2-associated GI symptom, reported in up to 50% of patients in some studies [2]. Presentation of SARS-CoV-2-associated diarrhea is

typically mild and characterized by loose or watery stools [2], but it can be more severe, with 18–30 diarrhea stools per day reported in some patients [3]. Also of note is that SARS-CoV-2 has been detected in fecal samples of COVID-19 patients with negative nasopharyngeal swabs [4], suggesting prolonged fecal–oral transmission as a plausible route of infection [5].

The pathogenesis of SARS-CoV-2-associated diarrhea is still under investigation. SARS-CoV-2 needs angiotensin-converting enzyme 2

* Corresponding author.

E-mail address: alfguari@unina.it (A. Guarino).

<https://doi.org/10.1016/j.heliyon.2022.e10246>

Received 21 December 2021; Received in revised form 25 February 2022; Accepted 5 August 2022

2405-8440/© 2022 Published by Elsevier Ltd. This is an open access article under the CC BY-NC-ND license (<http://creativecommons.org/licenses/by-nc-nd/4.0/>).

(ACE2) and transmembrane protease serine 2 (TMPRSS2) to enter enterocytes (sites of viral replication) after spike protein binding, cleavage, and internalization [6]. Both are localized on the apical surface of the human GI epithelium, with a high density in the distal tract [7, 8]. Typically, the pathophysiology of diarrhea involves one of two distinct mechanisms. The first is characterized by cytopathic damage often leading to cell death, a reduction in the digestive-absorptive surface and passive water flux into the intestinal lumen driven by unabsorbed nutrients, resulting in osmotic diarrhea. The second is characterized by a functional (rather than structural) pathogenic mechanism, and involves active ion secretion triggered by enterotoxins, which influences ion transport. It was initially proposed that cell death may be the pathogenic mechanism implicated in SARS-CoV-2-associated diarrhea as a consequence of SARS-CoV-2 entry and replication within enterocytes [9]. However, although there is evidence of invasion and destruction by actively replicating SARS-CoV-2 in some non-intestinal cell lines (e.g., Vero E6 cells), minimal cytopathic effects were observed in investigations of human-derived intestinal (Caco-2) cells [10]. Further, an ex vivo study showed that SARS-CoV-2 replicates less efficiently and induces less cytopathology than SARS-CoV in human intestinal tissue, but considering the short experimental infection time (24 h) a role for cytopathology in GI symptoms development cannot be excluded [11].

In the absence of clear causal evidence of structural damage in patients with SARS-CoV-2-associated diarrhea, a functional pathology could be implicated. This hypothesis is supported by evidence of virus-induced dysfunction of ACE2 receptors, leading to an imbalance in membrane ion channels (i.e., dysfunction in Na^+ -dependent glucose transporter [8] and Na^+/H^+ exchanger and neutral amino acid transporter [12] mechanisms, and in Ca^{2+} -activated Cl^- channels [CaCC] [13]). SARS-CoV-2 has also been shown to induce the production of reactive oxygen species (ROS) [14], suggesting a pathogenic mechanism potentially involving alteration of the intracellular redox state and promotion of chloride secretion in enterocytes, as observed for rotavirus [15]. Alterations of gut microbiota may also contribute to SARS-CoV-2-associated diarrhea [9], as could the prolonged presence of SARS-CoV-2 in the GI tract. Indeed, pediatric patients affected by Multisystem Inflammatory Syndrome (MIS-C), a later complication of COVID-19, showed persistent fecal viral shedding and an alteration in gut permeability, leading to trafficking of SARS-CoV-2 antigens into the bloodstream with consequent systemic hyperinflammation [16].

We previously developed a model of rotavirus-associated diarrhea, describing the sequence of the underlying pathogenic functional and structural viral effects. Briefly, rotavirus induced a sequence of events leading to diarrhea, including early electrogenic chloride secretion via its nonstructural protein 4 (NSP4) enterotoxin followed by cytotoxic damage. These effects were identifiable in vitro by electrical parameters in polarized intestinal cells, with the initial electrogenic chloride secretion being characterized by an increase in the intensity of the short-circuit current (*I*_{sc}), and cytotoxic damage being detectable by transepithelial electrical resistance (TEER) in Ussing chambers [15]. This in vitro model has been used to investigate the pathophysiology of diarrhea associated with a number of enteric pathogens and also the mechanisms of action of a number of anti-diarrheal agents (e.g., modified oral rehydration solutions [17], probiotics [15], and dioctahedral smectite [diosmectite] [18]).

In the present study, we used this experimental model of rotavirus-associated diarrhea to investigate the pathogenic effects of a viral preparation of SARS-CoV-2 and the pure spike protein in vitro using Caco-2 cells, and ex vivo using human intestinal specimens. We then compared the results to those obtained for rotavirus (using the same model). Because diosmectite was shown to neutralize the effects of rotavirus in this model of secretory diarrhea [18], and has been included as a treatment option in several protocols for the management of COVID-19-associated diarrhea [19, 20, 21], we assessed the effect of diosmectite on the potentially pathogenic effects induced by SARS-CoV-2 and pure spike protein.

2. Results

2.1. Effect on ion secretion (In Vitro)

Addition of the heat inactivated (hi) SARS-CoV-2 preparation to Caco-2 cell monolayers resulted in a significant increase in *I*_{sc} compared with control cells, indicating ion flux ($P < .0001$). The effect was dose-dependent, with a lowest effective hiSARS-CoV-2 dose of 0.01 ng/mL (change in *I*_{sc} [ΔI_{sc}], $2.9 \pm 1.4 \mu\text{A}/\text{cm}^2$, $P < .0001$). Maximum *I*_{sc} increase was observed with a hiSARS-CoV-2 dose of 1 ng/mL (ΔI_{sc} , $4.1 \pm 2.0 \mu\text{A}/\text{cm}^2$, $P < .0001$). No further increase in *I*_{sc} was induced by viral doses greater than 1 ng/mL (Figure 1A).

The greatest electrical effect, indicated by the area under the curve (AUC) of the ΔI_{sc} -time plot, was similar for hiSARS-CoV-2 preparation doses of 1 ng/mL and 10 ng/mL, suggesting saturation beyond 1 ng/mL (Figure 1B).

An increase in *I*_{sc} was observed only when the hiSARS-CoV-2 preparation was added to the mucosal but not the serosal side of the Caco-2 cell monolayers (ΔI_{sc} , $0.5 \pm 0.8 \mu\text{A}/\text{cm}^2$, $P < .0001$; Figure 1C), indicating a polarized effect. To assess whether the electrical effect was dependent on anion secretion rather than cation absorption, experiments were performed using Cl^- -free Ringer's solution. The electrical effect was largely eliminated by use of Cl^- -free Ringer's solution (ΔI_{sc} , $0.6 \pm 1.1 \mu\text{A}/\text{cm}^2$) rather than the Cl^- -containing Ringer's solution control ($P < .0001$). Changes in *I*_{sc} was also strongly reduced by pretreatment of cells with the intracellular calcium chelator bis(2-aminophenoxy)ethane N,N,N',N'-tetraacetic acid/acetoxymethyl ester (BAPTA/AM; $0.2 \pm 1.2 \mu\text{A}/\text{cm}^2$, $P < .0001$). This effect is related to the activity of CaCC, considering the ability of CaCCinh-A01 to inhibit the secretory effect ($P < .0001$) (Figure 1C).

To define the role of spike protein in determining the electrical effect induced by hiSARS-CoV-2, we measured *I*_{sc} changes in response to addition of spike protein to the mucosal side of the Caco-2 cell monolayers. Addition of pure spike protein induced anion secretion with a maximal effective dose of 1 ng/mL (ΔI_{sc} , $2.7 \pm 1.2 \mu\text{A}/\text{cm}^2$, $P < .0001$; AUC, $84 \pm 41 \mu\text{A} \cdot \text{min}$, $P < .0001$). Higher doses of spike protein did not induce a further increase in effect (Figure 2A–B). Spike protein induced a smaller increase in *I*_{sc} than the hiSARS-CoV-2 preparation (Figure 3A). Peak effect on ion secretion (i.e., maximum ΔI_{sc}) occurred 45–50 min after addition of the hiSARS-CoV-2 preparation and after spike protein addition. Peak *I*_{sc} was sustained for 10–15 min before decreasing slowly (Figure 3B). The temporal pattern of electrical effect observed with the hiSARS-CoV-2 preparation was similar to that seen for the enterotoxic effect of rotavirus and NSP4 using the same model (Figure 3C); these findings are consistent with previously published data for rotavirus [15,17,18].

In both hiSARS-CoV-2 and spike protein experiments performed in Ussing chambers, the serosal addition of theophylline induced an increase of *I*_{sc} comparable to controls, indicating cell survival at the end of the experiment (Figure 4A).

2.2. Effects on cell viability and apoptosis (In Vitro)

The cell viability was assessed by trypan blue staining. One hour after exposure to the hiSARS-CoV-2 preparation and spike protein, the number of viable cells were comparable in both groups compared to untreated cells ($P > .05$) (Figure 4B).

The increase of intracellular cleaved caspase 3 was assessed by flow cytometry as a marker of apoptosis induction. As shown in Figure 5, cell treatment with hiSARS-CoV-2 and spike protein did not activate the apoptotic pathway. Increase of cleaved caspase 3 level is instead shown by treatment with the cytotoxic agent Sodium Arsenite (ARS) at 1 h and further increase at 24 h.

2.3. Effects on epithelial integrity (In Vitro)

A reduction in transepithelial electrical resistance (TEER) indicates a breakdown in epithelial integrity. In this model, no cytotoxic effect was

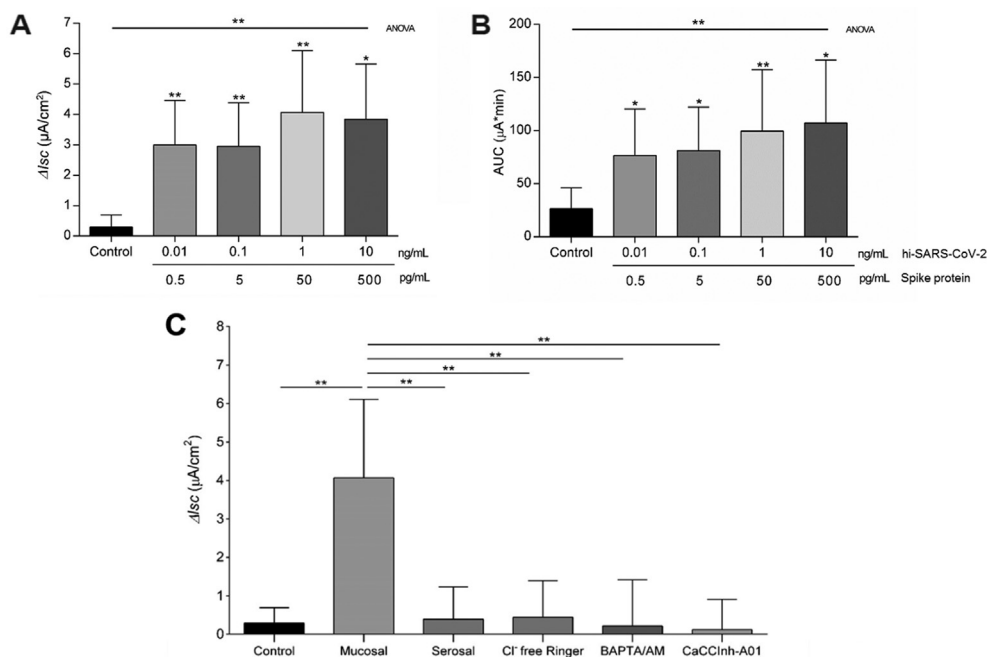


Figure 1. Effect of the hiSARS-CoV-2 preparation on transepithelial circuit current in Caco-2 cells. (A) hiSARS-CoV-2 induced a dose-dependent increase in I_{sc} with a trend towards saturation at 1 ng/mL. (B) Potency of the effect (assessed as the AUC) showed a dose-dependent increase. (C) No changes in I_{sc} were observed in the absence of hiSARS-CoV-2 or when hiSARS-CoV-2 was added to the serosal side (rather than the mucosal side) of the Caco-2 cell monolayer, or when chloride was removed from the Ringer's solution, or when the cells were pretreated with the calcium chelator BAPTA/AM or after mucosal addition of CaCClnh-A01. In (A) and (B) figures the second line of X-axis indicates the amount of spike protein contained in viral preparation for each concentration (about 5% of total protein content). * $P < .05$ vs control; ** $P < .0001$ vs control. ANOVA, analysis of variance; AUC, area under the curve of the ΔI_{sc} -time plot; BAPTA/AM, bis(2-aminophenoxy)ethane N,N,N',N'-tetra-acetic acid/acetoxymethyl ester; CaCClnh-A01, Ca^{2+} -activated Cl^- channel inhibitor A01; hiSARS-CoV-2, heat-inactivated SARS-CoV-2 preparation, I_{sc} , intensity of short-circuit current.

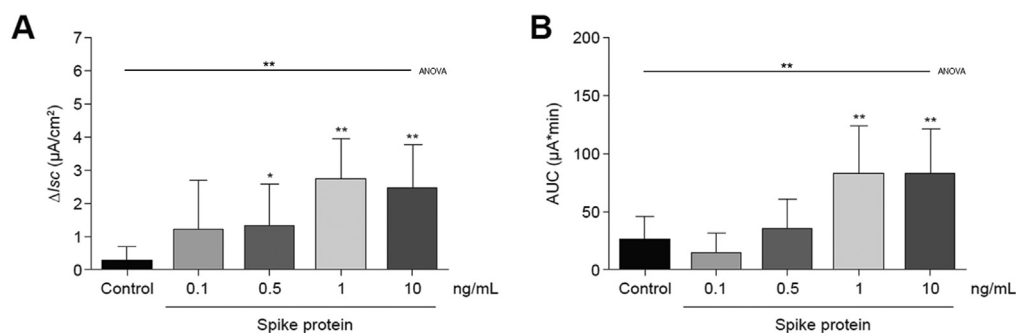


Figure 2. Electrogenic effects induced by spike protein in Caco-2 cells. (A) Spike protein induced a dose-dependent increase in I_{sc} with effect saturation at a dose of 1 ng/mL. (B) The potency of the effect (assessed as the AUC) showed a dose-dependent increase with a saturation pattern reached at a dose of 1 ng/mL. * $P < .05$ vs control; ** $P < .0001$ vs control. ANOVA, analysis of variance; AUC, area under the curve of the ΔI_{sc} -time plot; I_{sc} , intensity of short-circuit current.

observed for the hiSARS-CoV-2 preparation or the spike protein. This absence of effect was maintained over 72 h following exposure (Figure 6). The lack of apparent effect of hiSARS-CoV-2 or spike protein on epithelial integrity (as judged by TEER measurements) was consistent with that seen for NSP4 in the model of rotavirus-associated secretory diarrhea, but contrasted with that for living rotavirus in the same model, which showed a progressive TEER decrease from 24 h after incubation; these findings are consistent with previously published data [15,17].

2.4. Effects on electrical parameters in human intestinal specimens (ex vivo)

To assess the reproducibility of the results of the in vitro model in human intestinal cells, we repeated the experiments using human specimens of colonic mucosa in Ussing chambers. The ex vivo results were similar to those observed in the Caco-2 cells, although higher doses of the hiSARS-CoV-2 preparation and spike protein were required to achieve similar, statistically significant changes in I_{sc} (100 ng/mL) (Figure 7).

2.5. Effects on intestinal epithelial oxidative stress (In Vitro)

To test the hypothesis that the enterotoxic effect induced by SARS-CoV-2 involves oxidative stress, intracellular levels of ROS were

evaluated in Caco-2 cells stimulated with the hiSARS-CoV-2 preparation (1 μ g/mL) and pure spike protein (1 μ g/mL). A 2.5–3-fold increase in ROS was observed as early as 15 min after exposure to either preparation ($P < .0005$). For the hiSARS-CoV-2 preparation, ROS levels had returned to control values by 30 min, but reduced more gradually for spike protein, with peak value halving by 30 min and normalizing completely by 1 h, after exposure (Figure 8). Lower doses (1–100 ng/mL) were able to induce a minimal (1.5-fold) increase of ROS production 15 min after exposure to both preparations (Figure 9).

The effect on intracellular levels of ROS was consistent with previous findings with rotavirus and NSP4 [15]; although ROS increased more gradually with rotavirus and was sustained at 60 min.

2.6. Effects of Diosmectite on Electrogenic ion secretion and Oxidative Stress (In Vitro)

Pretreatment of both hiSARS-CoV-2 and spike protein with diosmectite (100 mg/mL for 1 h at 37 °C) virtually eliminated the effect on I_{sc} (Figure 10A). ROS production was also significantly reduced by pretreatment with diosmectite ($P < .05$) (Figure 10B), suggesting that diosmectite effectively abrogates the electrogenic ion secretion as well as oxidative stress effects induced by the hiSARS-CoV-2 preparation and the spike protein in this experimental model.

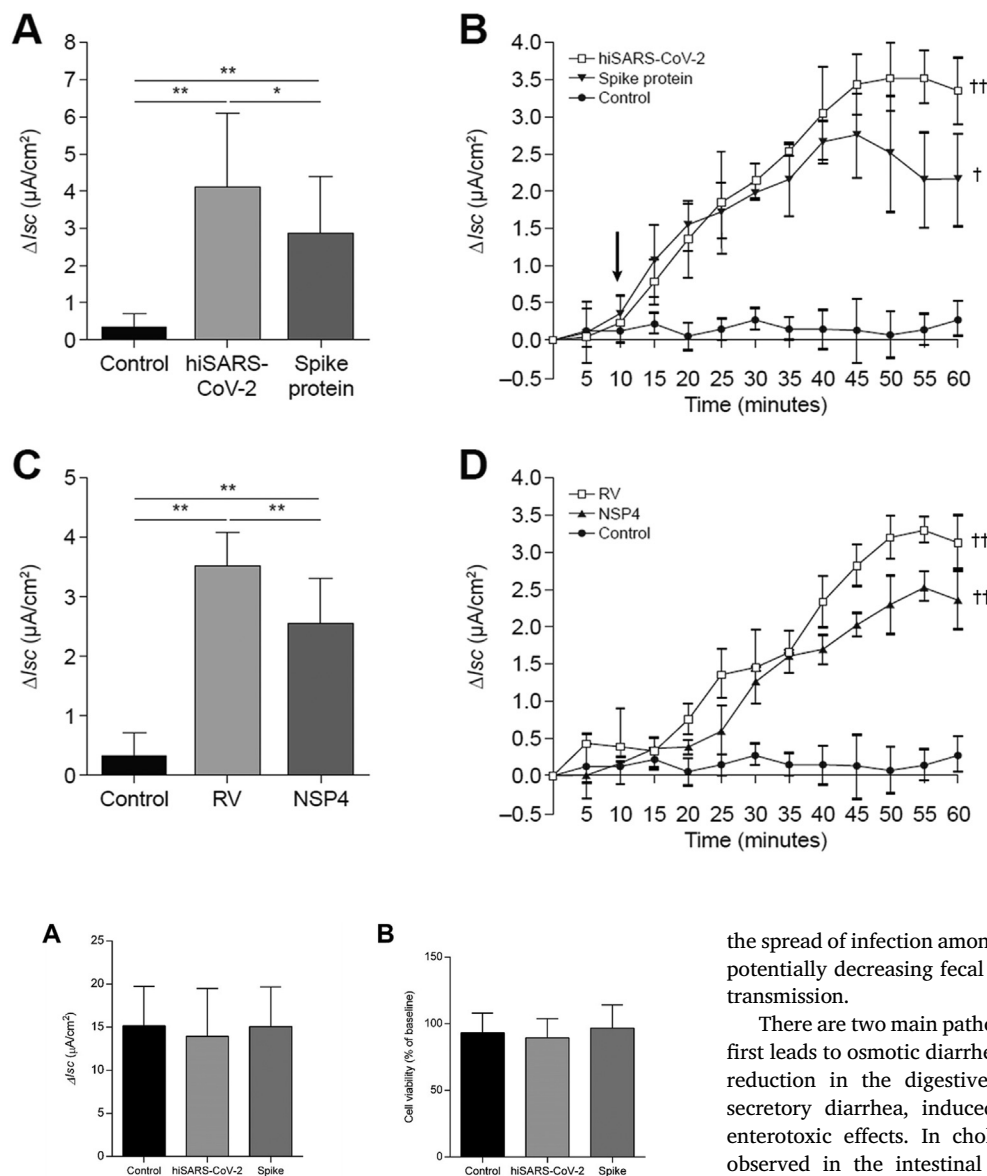


Figure 3. Electrogenic effects induced in Caco-2 cells by hiSARS-CoV-2 and spike protein. (A) Maximal change in I_{sc}. (B) Time-course analysis of I_{sc} (represents three experiments). I_{sc} was measured every 5 min for 60 min. Cells were stimulated at 10 min (arrow). (C) and (D) Electrogenic effects induced by rotavirus. The electrical effects induced by the hiSARS-CoV-2 preparation and spike protein were similar to those obtained with rotavirus and NSP4 using the same experimental model. **P* < .05 and ***P* < .0001 (t-test). †*P* < .05 and ††*P* < .01 (ANOVA). ANOVA, analysis of variance; I_{sc}, intensity of short-circuit current; NSP4, nonstructural viral protein 4; RV, rotavirus.

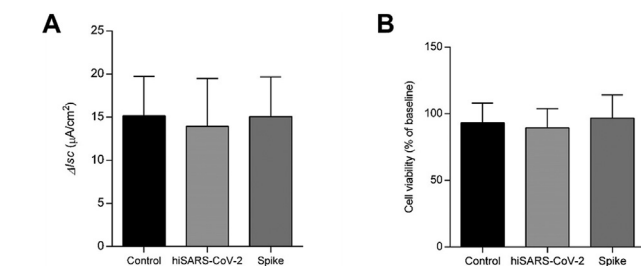


Figure 4. Caco-2 cell survival evaluated in Ussing chambers (A) and by trypan blue staining (B) after hi-SARS-CoV-2 and spike protein exposure (A) Cell survival in Ussing chambers was evaluated at the end of each experiment by measuring the electrical response to the serosal addition of the theophylline (5 mmol/L). The serosal addition of theophylline induced an increase of I_{sc} comparable to controls in cells previously treated with both hi-SARS-CoV-2 (1 ng/mL) and spike protein (1 ng/mL), indicating cell survival (B) Cell viability was assessed by trypan blue staining 1 h after exposure to the hiSARS-CoV-2 preparation (1 ng/mL) and spike protein (1 ng/mL). Untreated cells were used as negative controls. The data represent three separate experiments. No significant statistical differences were obtained. hiSARS-CoV-2, heat-inactivated SARS-CoV-2 preparation, I_{sc}, intensity of short-circuit current.

3. Discussion

The effects of SARS-CoV-2 on the respiratory tract are well recognized, but a substantial proportion of patients report GI complaints, most commonly diarrhea [2]. Although cases of SARS-CoV-2-associated diarrhea are often mild or moderate, they can be severe and require hospitalization and parenteral rehydration [2,3]. Also of importance for infection control are data suggesting that fecal shedding of the virus may be more prolonged than respiratory shedding and could contribute to potential risk of SARS-CoV-2 fecal-oral transmission [4, 5]. Viral removal from the GI lumen by drugs capable of binding viral particles may reduce

the spread of infection among enterocytes and the release of new virions, potentially decreasing fecal viral shedding time and stopping fecal-oral transmission.

There are two main pathophysiological mechanisms for diarrhea. The first leads to osmotic diarrhea, resulting from cell damage and a marked reduction in the digestive-absorptive surface. The second leads to secretory diarrhea, induced by active ion secretion in response to enterotoxic effects. In cholera, for example, little or no damage is observed in the intestinal epithelium, but massive electrogenic ion secretion is observed as reflected by changes of parameters in Ussing chambers. Rotavirus-associated diarrhea is caused by a combination of these osmotic and secretory diarrhea mechanisms [15, 22]. Active chloride secretion induced by NSP4 is observed in the early phase of rotavirus infection, followed by extensive epithelial damage; this aligns well with the clinical course in children.

The present work found evidence that SARS-CoV-2 induces anion secretion in a model of human intestinal cells. Spike protein is known to act through ACE2 binding in cooperation with TMPRSS2, allowing the virus to enter intestinal cells [6]. The density of ACE2 is greatest in the human body's small intestine, and ACE2 are located on the luminal side of polarized enterocytes [2]. Consistent with this topographical distribution, the electrical effect observed in our experiments was seen when the viral preparations were added to the mucosal but not the serosal side of polarized epithelium.

The increase in I_{sc} seen after exposure of the Caco-2 cells to the hiSARS-CoV-2 preparation and the pure spike protein is independent from cell death or apoptosis and is explained by an increased cation flux from the luminal side to the basolateral side of the cells, or (conversely) by enhanced anion secretion. Consistent with the pattern seen for other enterotoxins, such as rotavirus-NSP4, the effect on I_{sc} was eliminated by the removal of chloride and calcium and was dependent by CaCC. The electrogenic effect induced by the viral preparations was relatively rapid and dose dependent (until the point of saturation). Potency of the

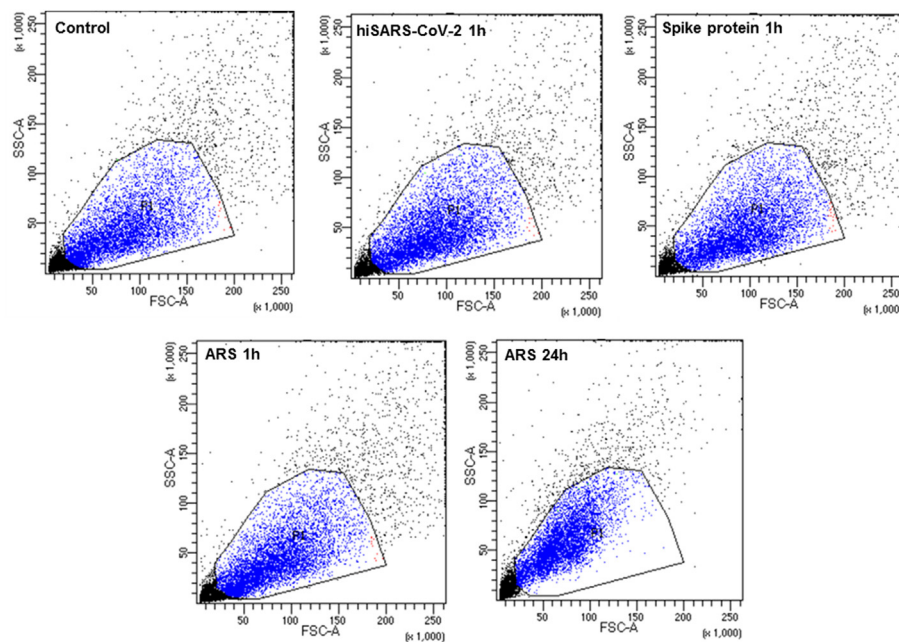


Figure 5. Cleaved caspase-3 levels in Caco-2 cells after hiSARS-CoV-2 and spike protein exposure. FACS analysis of Caco-2 untreated cells (Control) and treated with hiSARS-CoV-2, spike protein, and ARS. Representative flow cytometry plot indicating intracellular cleaved caspase-3 level. Figure is representative of three different experiments. ARS, sodium arsenite; FACS, fluorescence activated cell sorter; FITC-A, Fluorescein isothiocyanate area; FSC-A, forward scatter area; hiSARS-CoV-2, heat-inactivated SARS-CoV-2; SSC-A, side scatter area.

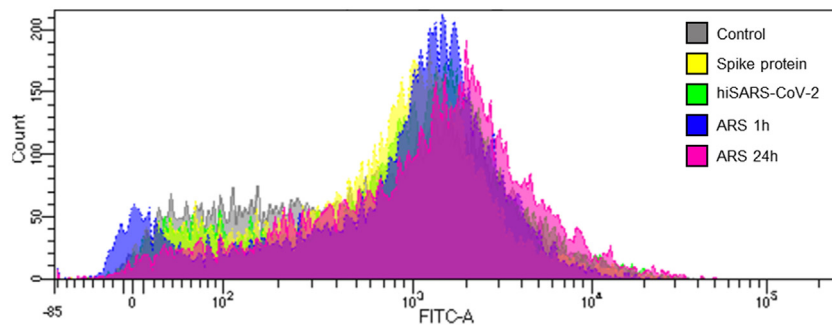
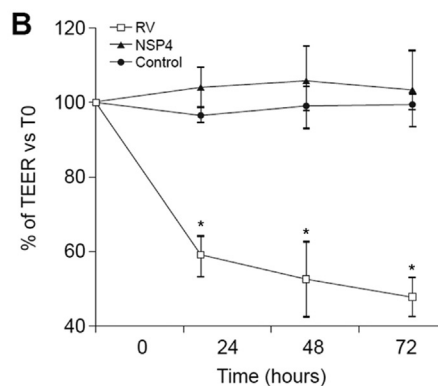
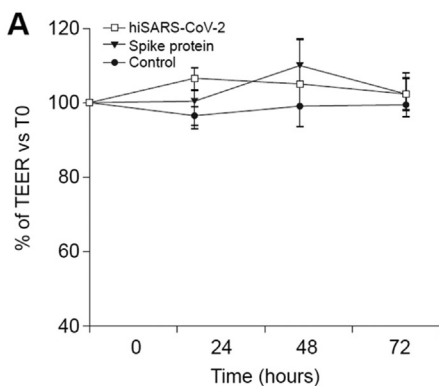


Figure 6. Transepithelial electrical resistance in Caco-2 cells following addition of hiSARS-CoV-2 or spike protein (A) and rotavirus or NSP4 (B). Cell monolayers were exposed to the hiSARS-CoV-2 preparation or spike protein at the mucosal side. The data are representative of three separate experiments. TEER results obtained with rotavirus and NSP4 are shown on the right for comparison. * $P < .01$ (ANOVA). ANOVA, analysis of variance; NSP4, nonstructural viral protein 4; RV, rotavirus; T0, TEER prior to exposure; TEER, transepithelial electrical resistance.



electrical effect was similar to that observed for rotavirus-NSP4 in the same experimental model, although comparisons were based on extrapolations from log-books of previous experiments rather than on parallel experiments of specific viral preparations. Data from the rotavirus experiments are consistent with previously published results [15,17,22].

The effects on *Isc* were also shown to be calcium-dependent, suggesting that calcium rather than cAMP or cGMP may be a mediator of the observed hiSARS-CoV-2-induced chloride secretion. The SARS-CoV-2 spike protein has been shown to lead to the activation of TMEM16 proteins, part of the CaCC family that is essential in syncytia formation from infected

pneumocytes [23]. Modulation of these transmembrane channels may also be involved in the development of secretory diarrhea [13]. Consistent with this, our results suggest that CaCC is implicated in SARS-CoV-2-induced anion secretion. These pathways have also been shown to be activated by NSP4 in a model of rotavirus-induced diarrhea [15].

The present analyses suggest that the spike protein, which is essential for SARS-CoV-2 binding and internalization, exhibits the typical features of an enterotoxin, similar to those of NSP4 in models of rotavirus-induced diarrhea [15,17]. Indeed, the results of our experiments with pure spike protein were consistent with those using the hiSARS-CoV-2 preparation,

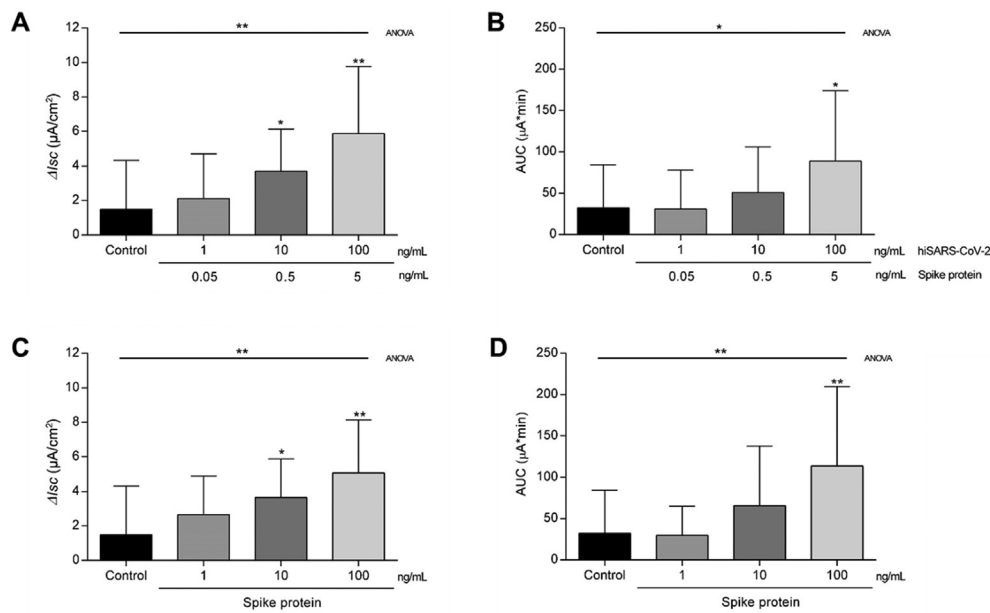


Figure 7. Electrogenic effects of hiSARS-CoV-2 (A-B) and spike protein (C-D) in human colonic specimens. Using chamber studies were performed, mounting human specimens of colonic mucosa after 1 h of incubation with different doses of hiSARS-CoV-2 (1–100 ng/mL) and spike protein (1–100 ng/mL). Change in *Isc* (A–C) and potency of the effect (assessed as the AUC) (B–D) showed a dose-dependent increase. In (A) and (B) figures the second line of X-axis indicates the amount of spike protein contained in viral preparation for each concentration (about 5% of total protein content). **P* < .05 vs control; ***P* < .005 vs control. ANOVA, analysis of variance; AUC, area under the curve of the ΔI_{sc} -time plot; hiSARS-CoV-2, heat-inactivated SARS-CoV-2; *Isc*, intensity of short-circuit current.

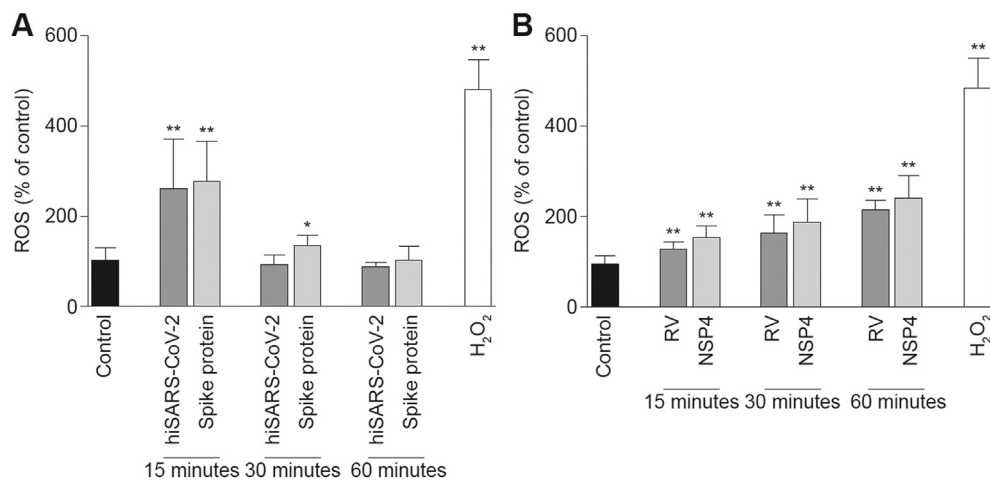


Figure 8. ROS induced in Caco-2 cells by hiSARS-CoV-2 or spike protein (A) and rotavirus or NSP4 (B). Intracellular ROS levels were evaluated by DCFH-DA fluorometry 15, 30, and 60 min after exposure to the hiSARS-CoV-2 preparation (1 μg/mL) and spike protein (1 μg/mL). Untreated cells and H₂O₂-treated cells were used as negative and positive controls, respectively. The data represent three separate experiments. Results obtained with rotavirus and NSP4 are shown on the right for comparison. ANOVA analysis of the time-course of hiSARS-CoV-2, spike protein, RV and NSP4 showed a *P* value < .0005 for all preparations. **P* < .05 vs control; ***P* < .0005 vs control. ANOVA, analysis of variance; DCFH-DA, 79-dichloro-fluorescein diacetate; hiSARS-CoV-2, heat-inactivated SARS-CoV-2; NSP4, nonstructural viral protein 4; ROS, reactive oxygen species; RV, rotavirus.

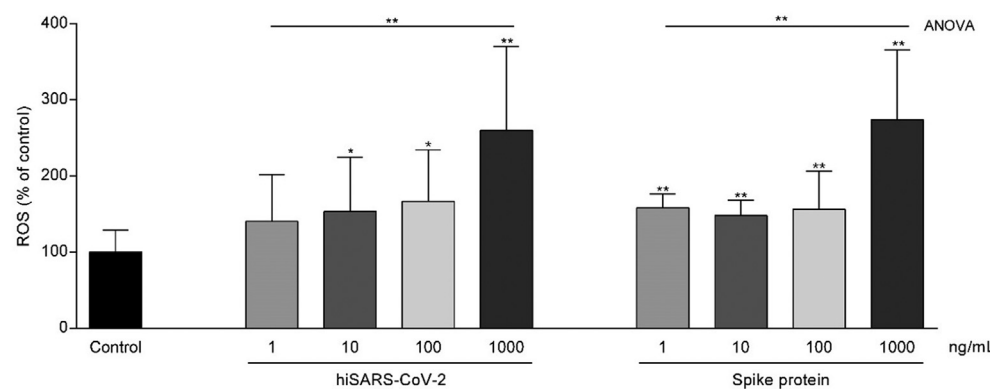


Figure 9. ROS induced in Caco-2 cells by different doses of hiSARS-CoV-2 and spike protein. Intracellular ROS levels were evaluated by DCFH-DA fluorometry 15 min after exposure to different doses of hiSARS-CoV-2 preparation (1–1000 ng/mL) and spike protein (1–1000 ng/mL). Untreated cells were used as negative controls. The data represent three separate experiments. The highest effect on ROS production was observed at 1 μg/mL for both preparations. **P* < .05 vs control; ***P* < .0005 vs control. ANOVA, analysis of variance; DCFH-DA, 79-dichloro-fluorescein diacetate; hiSARS-CoV-2, heat-inactivated SARS-CoV-2; ROS, reactive oxygen species.

indicating that spike protein is directly implicated in the enterotoxic effects of SARS-CoV-2. When we compared the effects on *Isc* and on the AUC of the ΔI_{sc} -time plot, the overall electrogenic effects were slightly higher for the hiSARS-CoV-2 preparation than for the pure spike protein.

Whether this is due to additional secretory moieties in the viral preparation or minor quantitative differences in the response of Caco-2 cells to the different preparations in a highly sensitive experimental system is unclear.

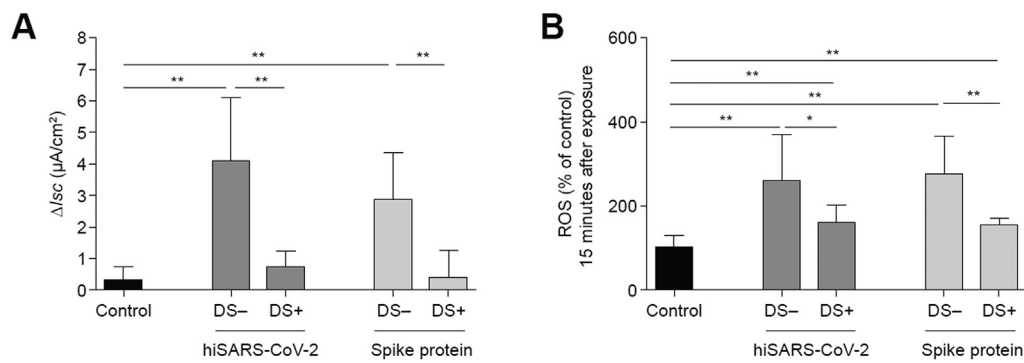


Figure 10. Effects of diosmectite on enterotoxicity and oxidative stress induced in Caco-2 cells by hiSARS-CoV-2 and spike protein. (A) Pretreatment with diosmectite (100 mg/mL) almost eliminated (DS⁺ vs DS⁻) the enterotoxic effects of the hiSARS-CoV-2 preparation and spike protein. (B) Pretreatment with diosmectite (100 mg/mL) strongly reduced ROS production (DS⁺ vs DS⁻) 15 min after exposure to the hiSARS-CoV-2 preparation and to spike protein. * $P < .05$; ** $P < .005$. DS, diosmectite; hiSARS-CoV-2, heat-inactivated SARS-CoV-2; I_{sc} , intensity of short-circuit current; ROS, reactive oxygen species.

Our experiments in human colonic specimens were consistent with the findings in the model, although the effects were generally less potent and higher concentrations of both viral preparation and spike protein were needed to achieve similar results. This is as expected when comparing experiments in intestinal cell lines with those in human specimens.

Intestinal cells showed a 2.5–3-fold increase in ROS production after exposure to the hiSARS-CoV-2 preparation and spike protein; increases in ROS production have also been reported in endothelial [24] and respiratory [25] cells after exposure to SARS-CoV-2. These findings are consistent with oxidative stress being a major factor in the development of acute respiratory distress syndrome and multiple organ dysfunction in acute COVID-19 [14]. The extent to which ROS increase is involved with ion secretion is not fully understood, but a similar pattern of ROS increase and ion secretion has been observed in a model of rotavirus-induced secretory diarrhea [15]. In addition, an increase of cytoplasmic Ca²⁺ concentration is induced by the oxidative stress [26]. These findings support the hypothesis that SARS-CoV-2, likely via the spike protein, exerts direct enterotoxic effects by modifying the cellular redox state, which leads to an increase of the intracellular Ca²⁺ concentration and to the subsequent CaCC activation. Given the early increase in ROS and rapid resolution (in 1 h) observed in our studies, oxidative stress may be a precursor to the pathogenic mechanisms involved in the SARS-CoV-2-induced diarrhea.

Recently, Donowitz et al. reported CaCC-dependent Cl⁻ secretion induced by spike protein in a preliminary *in vitro* study using human enteroids from healthy individuals [13]. Their findings differ from our results in that they only observed a spike-protein-induced electrical response and secretion in the presence of preexisting inflammation (induced by IL-6 plus IL-8 pretreatment), which suggests that an inflammatory response may be a prerequisite for secretion. Such differences in results may be due to the sensitivities of the experimental systems used in the respective studies and our use of a viral preparation of hiSARS-CoV-2 rather than virus-like particles.

In addition, we saw no short-term decrease (1 h) or long-term change (72 h) in the TEER of the Caco-2 cells, suggesting an absence of measurable damage to the mucosal architecture. A limitation of the study is the use of a heat-inactivated viral preparation instead of live SARS-CoV-2. Therefore, a structural damage induced by the live virus and measurable in terms of TEER reduction cannot be excluded. Nevertheless, this finding is consistent with the generally mild or moderate nature of SARS-CoV-2-associated diarrhea [2], although this is less true for rarer severe cases, such as those reported in children with MIS-C [27]. It may be that there are two distinct pathogenic mechanisms involved in SARS-CoV-2-induced diarrhea, the first being Cl⁻-dependent secretory diarrhea (similar to that involved in rotavirus-associated diarrhea, which causes more mild or moderate symptoms in patients with COVID-19), and the second being characterized by inflammation, as described by Donowitz et al. [13] (which results in more severe symptoms).

In addition to investigating the pathogenic mechanisms of SARS-CoV-2 and spike protein in our model of secretory diarrhea, we also assessed the

effect of diosmectite on the observed anion secretion and ROS production. Our selection of diosmectite for evaluation was informed by its inclusion within several protocols for the management of COVID-associated diarrhea [19, 20, 21]. It was also guided by *in vitro* studies demonstrating the effect of diosmectite in rotavirus-associated diarrhea [17], including ability to significantly reduce stool volume in children with rotavirus and acute watery diarrhea [28], and its inclusion as a recommended management option for acute gastroenteritis [29]. The doses of diosmectite used in our experimental model (100 mg/mL) are similar to those shown to be effective in the prevention of rotavirus-induced chloride secretion and oxidative stress [17]. Similar to its effect in rotavirus studies, diosmectite inhibited the chloride secretion and oxidative stress in Caco-2 cell monolayers induced by the hiSARS-CoV-2 preparation and spike protein. These effects could be linked to the properties of diosmectite and its ability to adsorb the virus and its active enterotoxin, preventing subsequent interactions with ACE2 on cell surfaces, as previously demonstrated with rotavirus and NSP4 [17].

Yonker et al. recently demonstrated that pediatric patients with MIS-C have high levels of spike antigenemia and persistent fecal SARS-CoV-2 shedding, suggesting that prolonged presence of SARS-CoV-2 in the gut could impair intestinal permeability targeting zonulin, thereby allowing SARS-CoV-2 antigens into the bloodstream and the development of systemic inflammation [16]. We hypothesize that the ability of diosmectite to bind SARS-CoV-2 may reduce viral load and virion release from infected cells within the gut, and may also reduce viral elimination time. Efficient viral removal from the GI tract has the potential to reduce infection risk, and the risk of systemic complications and MIS-C development.

In summary, our results provide novel insights into SARS-CoV-2-associated diarrhea. Similar to other infective diarrheas, particularly rotavirus diarrhea, SARS-CoV-2 induces chloride secretion through a calcium-dependent mechanism, suggesting the involvement of CaCCs. The secretory effect appears to be induced by the spike protein, which acts as an enterotoxin through mechanisms similar to those described for rotavirus gastroenteritis. Diosmectite reduced chloride secretion, likely via a trapping mechanism of the enterotoxic spike protein. Several reference centers have included diosmectite in their COVID-19 management protocols [19, 20, 21] and our results provide experimental support for consideration of its use for the management of COVID-associated diarrhea. In conclusion, SARS-CoV-2 should be considered as an enteric pathogen capable of inducing secretory diarrhea in children and adults and diosmectite could be listed among re-purposed drugs able to reduce SARS-CoV-2-induced effects.

4. Methods

4.1. Cell culture, specimens, virus and reagents

4.1.1. *In Vitro* model

Caco-2 cells derived from human colon carcinoma were used because of their ability to differentiate into enterocytes of the upper villus,

forming monolayers featuring ACE2 [30]. The cells (passage: 9–12) were grown in high glucose (4.5 g/L) Dulbecco's modified Eagle minimum essential medium (DMEM; Gibco, Thermo Fisher Scientific, Oxfordshire, UK) supplemented with fetal calf serum (FBS) (10%; Gibco), nonessential amino acids (1%), and penicillin-streptomycin (100 U/mL; Gibco). In all experiments using Caco-2 cell monolayers, each filter was seeded with a density of 5×10^5 cells/filter and grown for 18 days (with medium changed every 48 h).

A serum-free viral preparation of SARS-CoV-2 was obtained from the National Institute of Health (ISS, Rome, Italy) [31]. SARS-CoV-2 virus was amplified in Vero C1008 (Vero E6) cell culture. Cells were grown at 37 °C with 5% CO₂. Inoculation of Vero E6 cells with SARS-CoV-2 was carried out directly in DMEM. Medium harvested from infected cells 4 days after inoculation was clarified by centrifugation and heat inactivated at 56 °C for 30 min in a thermostatically-controlled water bath. Virus propagation and manipulation occurred in a BSL-3 laboratory setting at the National Institute of Health (ISS, Rome, Italy).

Liquid chromatography-mass spectrometry was used to confirm the total protein and spike protein concentrations in the hiSARS-CoV-2 preparation. The protein concentration of the hiSARS-CoV-2 preparation was 523 µg/mL; it contained 26 µg/mL of spike protein (i.e., approximately 5% of total protein).

The hiSARS-CoV-2 preparation and (separately) a commercial spike protein (RBD [V367F, SPD-S52H4]; ACRO Biosystems, Newark, DE, USA) were added to the apical or basolateral side of the Caco-2 cell monolayer at increasing doses in the absence or presence of diosmectite (Ipsen Consumer HealthCare, France). For diosmectite, the doses selected were the same as those used previously in experiments in rotavirus models of secretory diarrhea [18].

4.2. Ex vivo specimens

Human specimens of distal colon were obtained from 12 adult patients who underwent surgery for colon cancer. All specimens were taken from macroscopically normal areas of intestinal tissue and were confirmed as normal by histological analysis. The seromuscular layer was stripped to isolate colonic mucosa. Colonic mucosa specimens were washed with NaCl 0.9%, examined by stereomicroscope to exclude tissue necrosis, and treated with gentamicin 40 mg/mL to minimize bacterial contamination.

The hiSARS-CoV-2 preparation (1, 10 and 100 ng/mL) and spike protein (1, 10 and 100 ng/mL) were added to a DMEM with a high glucose concentration (4.5 g/L) supplemented with 0.5% FCS, 1% nonessential amino acids, 2% penicillin (50 mU/mL), and streptomycin (50 mg/mL). After 1 h of incubation at 37 °C with 5% CO₂, samples were mounted in Ussing chambers (filter area, 1.18 mm²) and *Isc* was monitored for 1 h. Untreated specimens incubated with medium in same conditions were used as controls.

4.3. Assessments

4.3.1. Ion transport

Caco-2 cells were grown on uncoated polycarbonate Transwell filters and used for intestinal transport studies 18 days after confluence. The filter area was 1.18 cm². Each filter was mounted in a Ussing chamber (Physiological Instruments, San Diego, CA, USA) between the mucosal and serosal compartments. Each compartment contained 5 mL of Ringer's solution with the following composition (in mmol/L): 114 NaCl; 5 KCl; 1.65 Na₂HPO₄; 0.3 NaH₂PO₄; 1.25 CaCl₂; 1.1 MgCl₂; 25 NaHCO₃, and 10 glucose. The buffer was constantly gassed with 95% O₂ and 5% CO₂, and was connected to a thermostat-regulated circulating pump to maintain a temperature of 37 °C.

Ion transport was studied by measuring modification in *Isc*, where an increase is an indication of active lumenally-directed anion secretion. As ΔI_{sc} is a precise marker of enterotoxic effects, maximal ΔI_{sc} was recorded as an indicator of mucosal ion secretion. The potency of the effect was

assessed as the integrated response of the Caco-2 cell monolayers under experimental conditions, evaluated as the AUC of the ΔI_{sc} -time plot, calculated by numerical integration with the baseline *Isc* subtracted.

The hiSARS-CoV-2 preparation was added to the mucosal and serosal side of Caco-2 cell monolayers at different doses (0.01–10 ng/mL of total protein content). Cell viability was evaluated at the end of each experiment by measuring the electrical response to the serosal addition of theophylline (5 mmol/L). To investigate the extent to which spike protein contributed to the electrical effect induced by the hiSARS-CoV-2 preparation, the experiments were repeated with the hiSARS-CoV-2 preparation replaced by pure spike protein at different doses (0.1–10 ng/mL). Untreated cells mounted in Ussing chamber were used as controls.

To investigate the role of Cl⁻ in the observed electrical response, Cl⁻ was substituted with SO₄²⁻ at an equimolar concentration. To investigate the role of Ca²⁺ in the electrical response, 1,2-bis(2-aminophenoxy) ethane N,N,N',N'-tetra-acetic acid/acetoxymethyl ester (BAPTA/AM 20 µM Enzo Life Sciences, Inc., NY, USA) was used as a calcium chelator. Caco-2 cells were pretreated with BAPTA/AM on both the mucosal and serosal sides 30 min before being mounted in Ussing chambers. The role of CaCC in *Isc* response was studied using the CaCC inhibitor A01 (10 µM, Tocris Bioscience, Bristol, UK), added to the mucosal side of Caco-2 cells 15 min before hiSARS-CoV-2 addition.

The results were compared with those of data on the electrical effects induced in Caco-2 cells infected by the simian rotavirus strain SA11 (multiplicity of infection, 25), or after the serosal addition of the rotavirus enterotoxin NSP4 (200 ng/mL) taken from log books of previous experiments; the methods used were as described in previous publications [15, 17, 18].

To test the effects of diosmectite on anion secretion, the hiSARS-CoV-2 preparation (1 ng/mL) and the pure spike protein (1 ng/mL) were pretreated with 100 mg/mL of diosmectite for 1 h at 37 °C followed by centrifugation. The cells were then stimulated using supernatants, as previously described.

4.4. Cell viability and apoptosis

Cell viability and apoptosis experiments were performed to ensure that electrical changes were linked to ion secretion and were independent of cell death, testing hiSARS-CoV-2 and spike protein at same doses (1 ng/mL) and conditions (1 h exposure at 37 °C) effective in Ussing chambers studies.

For cell viability experiment, 1×10^6 cells were seeded in 35 mm culture dishes for overnight attachment. Next day, cells were exposed to hiSARS-CoV-2 or spike protein for 1 h at 37 °C in serum-free medium. Cells exposed to fresh serum-free medium were used as control. At the end of incubation, cell viability was assessed by trypan blue dye exclusion assay, which is based on the microscopic quantitation of live cells (unstained) and dead cells (blue cytoplasm). Cells were automatically counted using the Countess Automated Cell Counter (Thermo Fisher Scientific, Milan, Italy).

To verify the apoptosis induction through caspase pathway activation we performed a quantitative analysis of the cleaved caspase 3 by Fluorescence activated cell sorter (FACS) analysis. Caco-2 cells were plated at a density of 2×10^4 cells/cm², after 24 h were treated with hiSARS-CoV-2 (1 ng/mL) and spike protein (1 ng/mL) for 1 h. Sodium Arsenite (ARS) (50 µM) treatment for 1 h and 24 h was used as positive control of apoptosis induction through caspase pathway activation. Cells were detached and suspended in 4% paraformaldehyde to prevent the cells forming clumps. After incubation for 20 min on ice, the cells were washed with 1 mL of IFA-TX buffer (Sodium chloride 0.9% at 4% fetal calf serum, 1% Hepes 1M, 0.1% Triton X-100), centrifugated at 300g for 5 min and suspended in primary antibody mix (anti-cleaved caspase-3 - cell signaling 9661) for 60 min on ice. Cells were then washed, re-suspended a 488 Alexa Fluor anti-rabbit secondary antibody mix (Invitrogen Corporation, Carlsbad, CA, USA) for 30 min on ice. After

centrifugation, cells were resuspended in PBS and filtered through 70 μm filcons (BD Biosciences Pharmingen, San Jose, CA, USA). The BD Biosciences FACS Aria III (BD Biosciences Pharmingen, San Jose, CA, USA) was used for analysis.

4.5. Epithelial integrity

Cytopathic effects of hiSARS-CoV-2 preparation and spike protein were assessed by measuring electrical resistance of Caco-2 cell monolayers mounted in Ussing chambers. TEER of cell monolayers grown on filters was measured using a Millicell-ERS resistance monitoring apparatus (Millipore, Merck Life Science S.r.l., Milan, Italy). The net TEER (in Ohms/cm²) was calculated by subtracting the background level from the actual value and then multiplying the resultant value obtained by the area of the filter (4.9 cm²). TEER was measured every 24 h for 3 days after mucosal addition of the hiSARS-CoV-2 preparation (100 ng/mL) and spike protein (100 ng/mL). Cells exposed to fresh serum-free medium were used as control.

4.6. Reactive oxygen species

ROS production was measured by 79-dichlorofluorescein diacetate (DCFH-DA, D6665; Sigma-Aldrich, St. Louis, MO, USA) spectrofluorometry. Caco-2 cells were grown in DMEM in 24-well plates for 18 days post confluence. Cell monolayers were treated with the hiSARS-CoV-2 (1 $\mu\text{g}/\text{mL}$) preparation and the spike protein (1 $\mu\text{g}/\text{mL}$) for 15, 30, and 60 min at 37 °C. The cells were then treated with DCFH-DA (20 μM) for 30 min at 37 °C in the dark. Intracellular ROS production was measured with a spectrofluorometer (SFM 25; Kontron Instruments, Tokyo, Japan). As positive controls, cells were incubated with H₂O₂ (10 mM) for 5 min and DCFH-DA for 30 min. As negative controls, cells were incubated with DCFH-DA in absence of stimuli. Same experiments were conducted after 15 min exposure to lower doses of hiSARS-CoV-2 and spike protein.

To assess the neutralization potential of diosmectite on ROS production, the hiSARS-CoV-2 preparation (1 $\mu\text{g}/\text{mL}$) and the pure spike protein (1 $\mu\text{g}/\text{mL}$) were preincubated with 100 mg/mL of diosmectite for 1 h at 37 °C followed by centrifugation. The cells were then stimulated using supernatants for 15 min, treated with DCFH-DA (20 μM) for 30 min at 37 °C in the dark, and tested by spectrofluorometry.

Statistical analysis

Descriptive results were reported as means and standard deviations. Between-group comparisons were performed by two-sided unpaired Student *t*-test and one-way analysis of variance (ANOVA), using Prism Software (GraphPad 6, San Diego, CA, USA). Bonferroni post-hoc test was performed for multiple testing correction. Statistical significance was defined as a *P* value of less than .05.

All experiments were repeated at least three times, and error bars indicate the standard deviation.

Ethics statement

The experiments with human specimens were conducted with the understanding and written consent of patients. The study protocol (No. 226/21) was approved by the Ethics Committee for Biomedical Activities, University of Naples Federico II, Naples, Italy.

Writing assistance

The authors thank Alison Chisholm, MPH, of Oxford PharmaGenesis, Oxford, UK, who provided medical writing and editorial support, which was sponsored by Ipsen in accordance with Good Publication Practice 3 (GPP3) guidelines.

Data transparency statement

Experimental data supporting the findings of this study are available from the corresponding author on request.

Declarations

Author contribution statement

Marco Poeta & Valentina Cioffi: Conceived and designed the experiments; Performed the experiments; Analyzed and interpreted the data; Wrote the paper.

Vittoria Buccigrossi: Conceived and designed the experiments; Analyzed and interpreted the data.

Francesco Corcione; Roberto Peltrini & Fabio Magurano: Contributed reagents, materials, analysis tools or data.

Angela Amoresano: Performed the experiments; Analyzed and interpreted the data.

Andrea Lo Vecchio & Eugenia Bruzzese: Analyzed and interpreted the data; Wrote the paper.

Maurizio Viscardi & Giovanna Fusco: Performed the experiments; Contributed reagents, materials, analysis tools or data.

Antonietta Tarallo & Carla Damiano: Performed the experiments; Analyzed and interpreted the data; Contributed reagents, materials, analysis tools or data.

Alfredo Guarino: Conceived and designed the experiments; Analyzed and interpreted the data; Wrote the paper.

Funding statement

This work was supported in part by Ipsen Consumer HealthCare, France. The funders had no role in the study design, data collection, analysis, and decision to publish. The sponsor was involved in the editing of the manuscript. No additional external funding was received for this study.

Data availability statement

Data will be made available on request.

Declaration of interest's statement

The authors declare no conflict of interest.

Additional information

No additional information is available for this paper.

Acknowledgements

The authors wish to thank Dr Melissa Baggieri, Dr Antonella Marchi, Dr Paola Bucci, Dr Merlin Nanayakkara for their technical support.

References

- [1] J. Zhang, S. Garrett, J. Sun, Gastrointestinal symptoms, pathophysiology, and treatment in COVID-19, *Genes Dis* 8 (4) (2021) 385–400.
- [2] K. Megyeri, Á. Dernovics, Z.I.I. Al-Luhaibi, A. Rosztóczy, COVID-19-associated diarrhea, *World J. Gastroenterol.* 27 (23) (2021) 3208–3222.
- [3] C. Han, C. Duan, S. Zhang, B. Spiegel, H. Shi, W. Wang, L. Zhang, R. Lin, J. Liu, Z. Ding, X. Hou, Digestive symptoms in COVID-19 patients with mild disease severity: clinical presentation, stool viral RNA testing, and outcomes, *Am. J. Gastroenterol.* 115 (6) (2020) 916–923.
- [4] L. Pan, M. Mu, P. Yang, Y. Sun, R. Wang, J. Yan, P. Li, B. Hu, J. Wang, C. Hu, Y. Jin, X. Niu, R. Ping, Y. Du, T. Li, G. Xu, Q. Hu, L. Tu, Clinical characteristics of COVID-19 patients with digestive symptoms in hubei, China: a descriptive, cross-sectional, multicenter study, *Am. J. Gastroenterol.* 115 (5) (2020) 766–773.
- [5] J. Hindson, COVID-19: faecal-oral transmission? *Nat. Rev. Gastroenterol. Hepatol.* 17 (5) (2020) 259.

- [6] M.G. Puoti, A. Rybak, F. Kiparissi, E. Gaynor, O. Borrelli, SARS-CoV-2 and the gastrointestinal tract in children, *Front Pediatr* 9 (2021) 617980.
- [7] I. Hamming, W. Timens, M.L. Bulthuis, A.T. Lely, G. Navis, H. van Goor, Tissue distribution of ACE2 protein, the functional receptor for SARS coronavirus. A first step in understanding SARS pathogenesis, *J. Pathol.* 203 (2) (2004) 631–637.
- [8] A. Kumar, M.A. Faiq, V. Pareek, K. Raza, R.K. Narayan, P. Prasoon, P. Kumar, M. Kulandhasamy, C. Kumari, K. Kant, H.N. Singh, R. Qadri, S.N. Pandey, S. Kumar, Relevance of SARS-CoV-2 related factors ACE2 and TMPRSS2 expressions in gastrointestinal tissue with pathogenesis of digestive symptoms, diabetes-associated mortality, and disease recurrence in COVID-19 patients, *Med. Hypotheses* 144 (2020) 110271.
- [9] C.A. Devaux, J.C. Lagier, D. Raoult, New insights into the physiopathology of COVID-19: SARS-CoV-2-Associated gastrointestinal illness, *Front. Med.* 8 (2021) 640073.
- [10] N. Wurtz, G. Penant, P. Jardot, N. Duclos, B. La Scola, Culture of SARS-CoV-2 in a panel of laboratory cell lines, permissivity, and differences in growth profile, *Eur. J. Clin. Microbiol. Infect. Dis.* 40 (3) (2021) 477–484.
- [11] H. Chu, J.F. Chan, Y. Wang, T.T. Yuen, Y. Chai, H. Shuai, D. Yang, B. Hu, X. Huang, X. Zhang, Y. Hou, J.P. Cai, A.J. Zhang, J. Zhou, S. Yuan, K.K. To, I.F. Hung, T.T. Cheung, A.T. Ng, I. Hau-Yee Chan, I.Y. Wong, S.Y. Law, D.C. Foo, W.K. Leung, K.Y. Yuen, SARS-CoV-2 induces a more robust innate immune response and replicates less efficiently than SARS-CoV in the human intestines: an ex vivo study with implications on pathogenesis of COVID-19, *Cell Mol Gastroenterol Hepatol* 11 (3) (2021) 771–781.
- [12] A.P. de Oliveira, A.L.F. Lopes, G. Pacheco, I.R. de Sá Guimarães Nôlêto, L.A.D. Nicolau, J.V.R. Medeiros, Premises among SARS-CoV-2, dysbiosis and diarrhea: walking through the ACE2/mTOR/autophagy route, *Med. Hypotheses* 144 (2020) 110243.
- [13] M. Donowitz, C.M. Tse, K. Dokladny, M. Rawat, I. Horwitz, C. Ye, A. Kell, R. Lin, S. Lee, C. Guo, S.J. Tsai, A. Cox, S. Gould, J. In, S. Bradfute, N.C. Zachos, O. Kovbasnjuk, SARS-CoV-2 Induced Diarrhea Is Inflammatory, Ca²⁺-Dependent and Involves Activation of Calcium Activated Cl Channels, *bioRxiv* (2021), 2021.04.27.441695.
- [14] A.M. Barciszewska, Elucidating of oxidative distress in COVID-19 and methods of its prevention, *Chem. Biol. Interact.* 344 (2021) 109501.
- [15] V. Buccigrossi, G. Laudiero, C. Russo, E. Miele, M. Sofia, M. Monini, F.M. Ruggeri, A. Guarino, Chloride secretion induced by rotavirus is oxidative stress-dependent and inhibited by *Saccharomyces boulardii* in human enterocytes, *PLoS One* 9 (6) (2014) e99830.
- [16] L.M. Yonker, T. Gilboa, A.F. Ogata, Y. Senussi, R. Lazarovits, B.P. Boribong, Y.C. Bartsch, M. Loisel, M.N. Rivas, R.A. Porritt, R. Lima, J.P. Davis, E.J. Farkas, M.D. Burns, N. Young, V.S. Mahajan, S. Hajizadeh, X.L.H. Lopez, J. Kreuzer, R. Morris, E.E. Martinez, I. Han, K. Griswold Jr., N.C. Barry, D.B. Thompson, G. Church, A.G. Edlow, W. Haas, S. Pillai, M. Arditi, G. Alter, D.R. Walt, A. Fasano, Multisystem inflammatory syndrome in children is driven by zonulin-dependent loss of gut mucosal barrier, *J. Clin. Invest.* 131 (14) (2021).
- [17] V. Buccigrossi, A. Lo Vecchio, E. Bruzzese, C. Russo, A. Marano, S. Terranova, V. Cioffi, A. Guarino, Potency of oral rehydration solution in inducing fluid absorption is related to glucose concentration, *Sci. Rep.* 10 (1) (2020) 7803.
- [18] V. Buccigrossi, C. Russo, A. Guarino, M.B. de Freitas, A. Guarino, Mechanisms of antiarrhoeal effects by diosmectite in human intestinal cells, *Gut Pathog.* 9 (2017) 23.
- [19] R. Mao, Expert consensus on diagnosis and treatment of COVID-19 digestive system, *Chin. J. Nat. Med.* 100 (2000).
- [20] Lombardy Ministry for Health, Acts of guidance for integrated hospital-territory management for assistance to COVID-19 or suspected patients. <https://www.regione.lombardia.it/wps/portal/istituzionale/HP/istituzione/Giunta/sedute-del-ibere-giunta-regionale/DettaglioDelibere/delibera-3876-legislatura-11>, 2020. (Accessed 16 August 2022).
- [21] Republic. MoHotC. Diarrhea manual of care for patients with COVID-19 hospitalized in a standard ward. June 25, 2020. <https://www.infekce.cz/Covid2019/ManualPece1120p.pdf>. (Accessed 16 August 2022).
- [22] G. De Marco, I. Bracale, V. Buccigrossi, E. Bruzzese, R.B. Canani, G. Polito, F.M. Ruggeri, A. Guarino, Rotavirus induces a biphasic enterotoxic and cytotoxic response in human-derived intestinal enterocytes, which is inhibited by human immunoglobulins, *J. Infect. Dis.* 200 (5) (2009) 813–819.
- [23] L. Braga, H. Ali, I. Secco, E. Chiavacci, G. Neves, D. Goldhill, R. Penn, J.M. Jimenez-Guardeño, A.M. Ortega-Prieto, R. Bussani, A. Cannatà, G. Rizzari, C. Collesi, E. Schneider, D. Arosio, A.M. Shah, W.S. Barclay, M.H. Malim, J. Burrone, M. Giacca, Drugs that inhibit TMEM16 proteins block SARS-CoV-2 spike-induced syncytia, *Nature* 594 (7861) (2021) 88–93.
- [24] K. Meyer, T. Patra, Ray R. Vijayamahantes, SARS-CoV-2 spike protein induces paracrine senescence and leukocyte adhesion in endothelial cells, *J. Virol.* (2021) Jvi0079421.
- [25] R. Cecchini, A.L. Cecchini, SARS-CoV-2 infection pathogenesis is related to oxidative stress as a response to aggression, *Med. Hypotheses* 143 (2020) 110102.
- [26] G. Ermak, K.J.A. Davie, Calcium and oxidative stress: from cell signaling to cell death, *Mol. Immunol.* 38 (10) (2002) 713–721.
- [27] L.R. Feldstein, M.W. Tenforde, K.G. Friedman, M. Newhams, E.B. Rose, H. Daput, V.L. Soma, A.B. Maddux, P.M. Mourani, C. Bowens, M. Maamari, M.W. Hall, B.J. Riggs, J.S. Giuliano Jr., A.R. Singh, S. Li, M. Kong, J.E. Schuster, G.E. McLaughlin, S.P. Schwartz, T.C. Walker, L.L. Loftis, C.V. Hobbs, N.B. Halasa, S. Doymaz, C.J. Babbitt, J.R. Hume, S.J. Gertz, K. Irby, K.N. Clouser, N.Z. Cvijanovich, T.T. Bradford, L.S. Smith, S.M. Heidemann, S.P. Zackai, K. Wellnitz, R.A. Nofziger, S.M. Horwitz, R.W. Carroll, C.M. Rowan, K.M. Tarquinio, E.H. Mack, J.C. Fitzgerald, B.M. Coates, A.M. Jackson, C.C. Young, M.B.F. Son, M.M. Patel, J.W. Newburger, A.G. Randolph, Characteristics and outcomes of US children and adolescents with Multisystem inflammatory syndrome in children (MIS-C) compared with severe acute COVID-19, *JAMA* 325 (11) (2021) 1074–1087.
- [28] C. Dupont, J.L. Foo, P. Garnier, N. Moore, H. Mathie-Fortunet, E. Salazar-Lindo, Oral diosmectite reduces stool output and diarrhea duration in children with acute watery diarrhea, *Clin. Gastroenterol. Hepatol.* 7 (4) (2009) 456–462.
- [29] A. Guarino, S. Ashkenazi, D. Gendrel, A. Lo Vecchio, R. Shamir, H. Szajewska, European society for pediatric gastroenterology, hepatology, and nutrition/ European society for pediatric infectious diseases evidence-based guidelines for the management of acute gastroenteritis in children in Europe: update 2014, *J. Pediatr. Gastroenterol. Nutr.* 59 (1) (2014) 132–152.
- [30] S. Kumar, P. Sarma, H. Kaur, M. Prajapat, A. Bhattacharyya, P. Avti, N. Sehkhari, H. Kaur, S. Bansal, S. Mahendiratta, V.M. Mahalmani, H. Singh, A. Prakash, A. Kuhad, B. Medhi, Clinically relevant cell culture models and their significance in isolation, pathogenesis, vaccine development, repurposing and screening of new drugs for SARS-CoV-2: a systematic review, *Tissue Cell* 70 (2021) 101497.
- [31] F. Magurano, M. Baggieri, A. Marchi, G. Rezza, L. Nicoletti, SARS-CoV-2 infection: the environmental endurance of the virus can be influenced by the increase of temperature, *Clin. Microbiol. Infect.* 27 (2) (2021) 289, e5–e7.